KfK 4169
Oktober 1986

Progress in Composites: Microstructure-Thermomechanical-Property Correlations of Two-phase and Porous Materials

G. Ondracek
Institut für Material- und Festkörperforschung

Kernforschungszentrum Karlsruhe

KERNFORSCHUNGSZENTRUM KARLSRUHE

Institut für Material- und Festkörperforschung

KfK 4169

Progress in Composites:

Microstructure-Thermomechanical-Property Correlations of Two-phase and Porous Materials

G. Ondracek

Kernforschungszentrum Karlsruhe GmbH, Karlsruhe

Materials Chemistry and Physics, 15 (1986) 281–313

MICROSTRUCTURE-THERMOMECHANICAL-PROPERTY CORRELATIONS OF TWO-PHASE AND POROUS MATERIALS

G. ONDRACEK

Postfach 3640 - IMF, Kernforschungszentrum und Universität, 7500 Karlsruhe (F.R.G.)

ABSTRACT

The paper basically deals with the aim, to a get a better scientific insight into the effects of microstructure and properties of multi-phase and porous materials and to use the results technologically for tailoring those materials. First the theory of microstructure-property correlations including both, the bound concept and the model concept, is described using conductivity and Youngs modulus of elasticity as property examples. Since in the frame of the theoretical derivation no fitting factors have been permitted to be introduced into the bound equations and constitutive equations the determination of the microstructural factors by quantitative microstructural analysis is demonstrated in the second part of the contribution. By comparing measured and calculated property values for porous ceramics, graphite and metals as well as cermets, metal-polymer and polymer-ceramic-composites the equations are tested for engineering conditions. Finally the dependences of the thermal conductivity and Youngs modulus of elasticity on porosity are used to predict the thermal shock resistance of porous glass and to compare the results with experimental values.

INTRODUCTION

The present paper is written as an introductory guideline to the subject and not as a final report. Comprehension is endeavoured, details refer to the references. Simple spoken style has been choosen due to a workshop lecture, certainly not perfect in language, neither in expression nor in grammar and syntax, but - this I do hope - useful as an understandable basis for discussion.

0254-0584/86/$3.50

Originally the starting point for us to enter the problem of microstructure-property-relations was not only to get a better scientific insight into the behaviour of multiphase materials but also the need to develop or 'construct' - a type of tailor-made-materials in order to substitute less available or ecologically suspicious constituents in conventional engineering materials.

For doing so we first had to find out about the theoretical correlation between microstructure and properties of multiphase materials. In this context microstructure refers to the geometry and geometrical arrangement of the materials constituents and is already clearly separated from the 'atomistic structure', say the materials composition, the X-ray structure as well as the macrostructure in a one-dimensional scale (Fig. 1) [20].

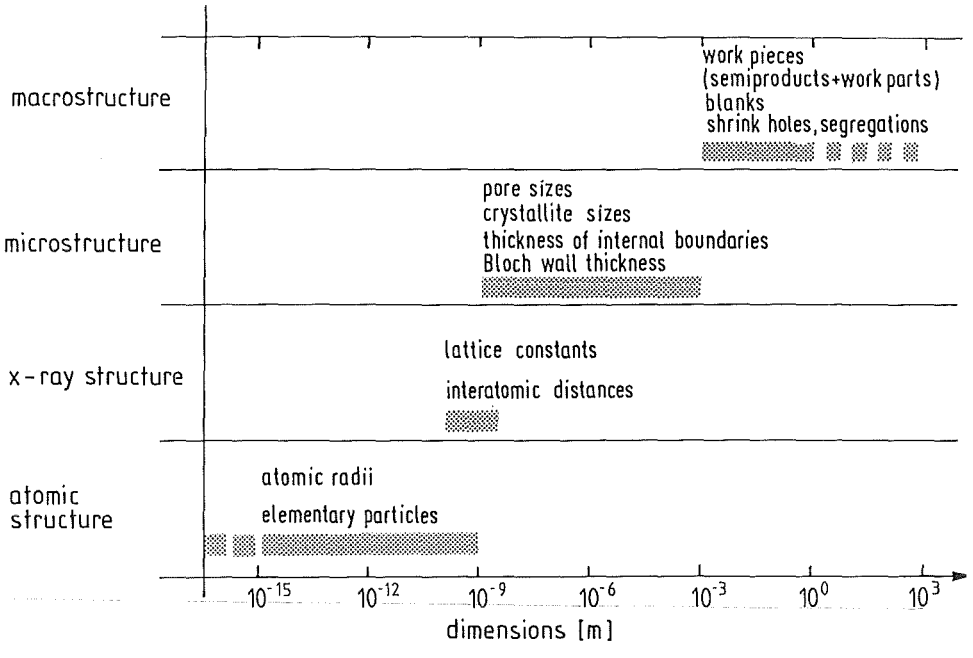

Fig. 1. Subdivision of materials structure.

Treating properties in their relation to microstructure we found out - also from the literature - that the derivation of certain properties is based on the same principles and leads to identical results for all of them [1,2,3]. So for example, the electrical and thermal conductivity, the electrical permittivity as well as the magnetic permeability altogether appear in so called field equations of the same type, which form the basis for the derivation of their - identical - microstructural dependences. This is why we may treat them as one group. Other property groups are given in Fig. 2. The term technical properties refers to those, which are of special practical interest and consist theoretically of a mathematical combination of - for instance - field properties and mechanical properties. An example in this context is the thermal shock resistance equation [4]

$$R_{TS} = \text{const.} \frac{R_m}{\alpha_{th}} \cdot \frac{\Phi_{th}}{E} (1-\nu) \qquad (1)$$

STRUCTURE	MATERIALS and PROPERTIES
atomic structure	thermodynamic properties
X-ray structure	field properties
microstructure	mechanical properties
macrostructure	technical properties

Fig. 2. Structure and property groups.

for brittle materials as carbon or glass which contains the ratio between thermal conductivity (ϕ_{th}) and Young's modulus (E) as a governing term (R_{TS} = thermal shock resistance; R_m = rupture strength; α_{th} = coefficient of thermal expansion; ν = Poisson ratio). As a consequence, if we want to improve the thermal shock behaviour of glass or ceramics by constructing cermet-composites we have to do with this ratio between thermal conductivity and Young's modulus (Fig. 3), being rather different for metals and ceramics, which form the constituents in cermets. And we have to know how the microstructure of such a ceramic-metal-combination effects the conductivity and Youngs Modulus. This is why I now turn to the theoretical derivation of microstructure-property equations

- for field properties including conductivity and
- for elastic properties as Youngs modulus.

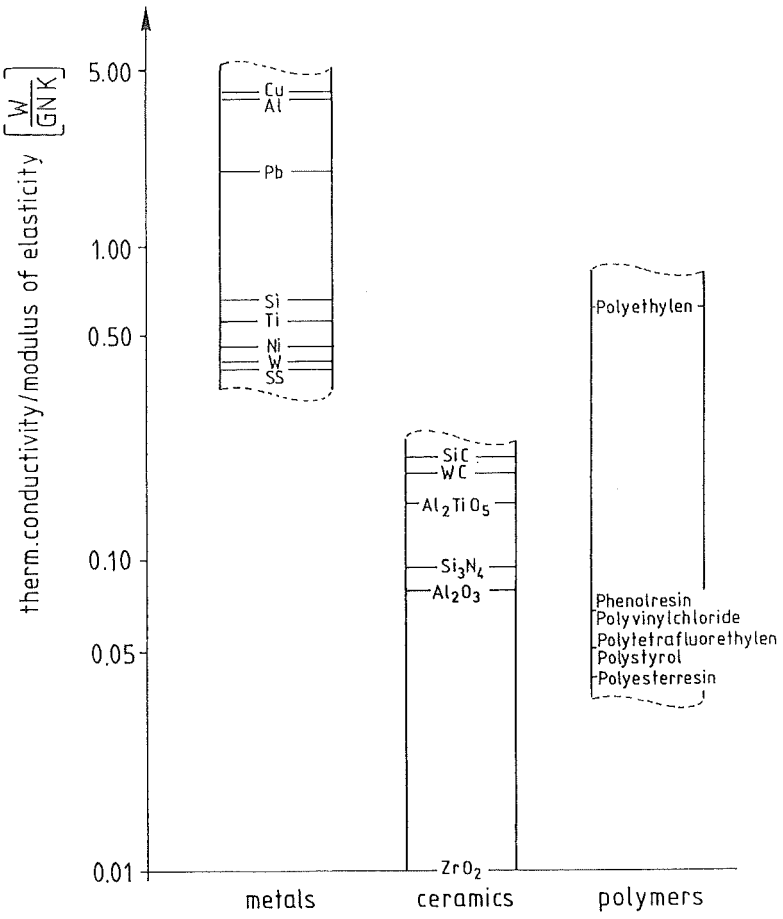

Fig. 3. Thermal conductivity/Young's modulus for metals, ceramics and polymers.

THEORY OF MICROSTRUCTURE-PROPERTY-CORRELATIONS

Conductivity

Bound concept

To obtain the microstructure-field property interrelationship quantitatively on a theoretical basis two concepts exist [1]

- the bound concept and
- the model concept.

In case of the bound concept the constituents of the two-phase material are considered separately in the respective electrical, magnetic or temperature field as shown in Fig. 4 [5,6].

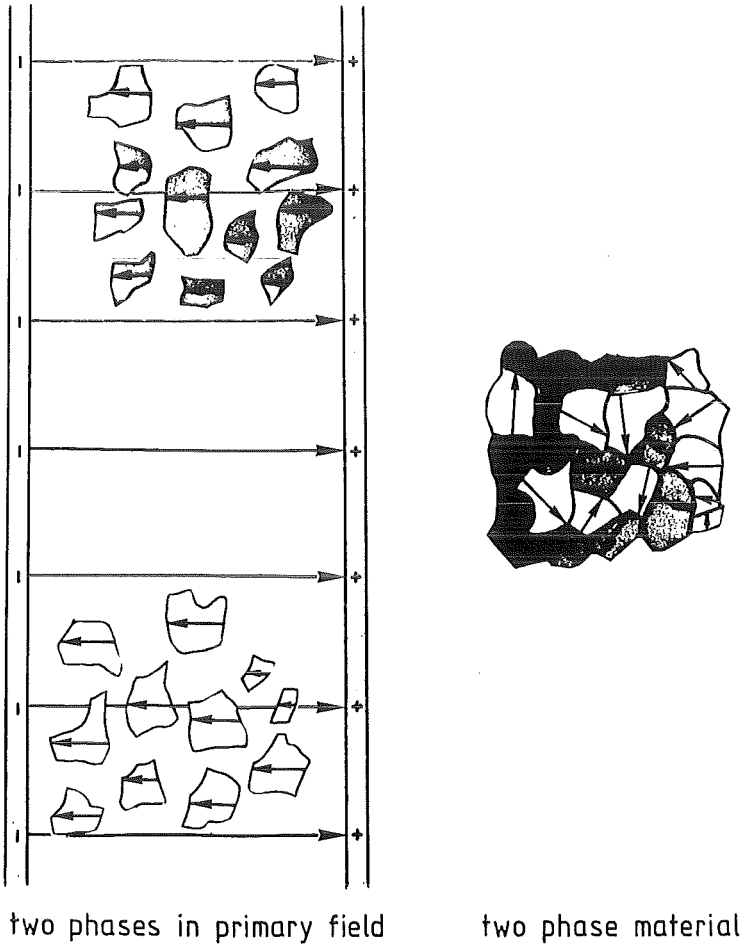

Fig. 4. Bound concept schematically.

By field influence the materials take up field energy, where these energy terms behave additively, when composing the components to one piece. The resulting energy equation provides two solutions for the effective field property; the solutions themselves depend on the microstructural information to be available or assumed to be correct as limiting conditions:

- for example supposing or knowing nothing more, than that the material is two-phased one obtains an utmost upper (ϕ^{I}_{C}) and a lower value (ϕ_{IC}) bounding all possible property quantities in between I order bounds (Fig. 5) so called for referring to one single assumption: the number of phases

	lower bounds	upper bounds
I. order	$\varphi_{IC} = \frac{\varphi_1 \varphi_2}{c_2\varphi_1 + (1-c_2)\varphi_2}$	$\varphi^{I}_{C} = c_2\varphi_2 + (1-c_2)\varphi_1$
II. order	$\varphi_{IIC} = \varphi_1 \frac{3\varphi_2 + 2(1-c_2)(\varphi_1-\varphi_2)}{3\varphi_1 - (1-c_2)(\varphi_1-\varphi_2)}$	$\varphi^{II}_{C} = \varphi_2 \frac{3\varphi_1 + 2c_2(\varphi_2-\varphi_1)}{3\varphi_2 - c_2(\varphi_2-\varphi_1)}$
	$\varphi_1 < \varphi_2$	
III. order	$1-c_D = \frac{\varphi_{IIIC} - \varphi_D}{\varphi_M - \varphi_D} \frac{\varphi_M + 2\varphi_D}{\varphi_{IIIC} + 2\varphi_D}$	$1-c_D = \frac{\varphi^{III}_{C} - \varphi_D}{\varphi_M - \varphi_D} \sqrt[3]{\frac{\varphi_M}{\varphi^{III}_{C}}}$
	$\varphi_D < \varphi_M$	

Fig. 5. Bound equations (2÷7) of field properties (ϕ_1, ϕ_2 = field property values of phase 1,2; ϕ_M, ϕ_D = field property values of phase M,D; c_1, c_2, c_D = volume content of phase 1,2,D).

- another couple of equations represents closer II. order bounds ($\phi^{I,I}_{C}$, ϕ_{IIC}) being valid for materials with two microstructural informations: the material is two-phased and the material is isotropic.

- finally, knowing that the material is two-phased, isotropic and that one phase serves as a continous matrix-phase, whilst the other is included discontinuously we get even closer III order bounds (ϕ^{III}_{C}, ϕ_{IIIC}) due to three microstructural assumptions: the number of phases to be two; the type of microstructure to be a matrix phase type; the orientation of phases to be statistical, representing an isotropic material.

Plotting the results as concentration function for the conductivity of the two-phase material we obtain Fig. 6. Up to here I may say that the bound concept does not need definite geometrical assumptions. The bound equations - implicitely - refer to

- a definite number of phases (I order) and
- isotropic material (II order bounds) and
- a definite matrix phase structure (III order bounds)

but do not include any geometrically prescribed microstructural parameter. In so far the bound concept keeps closer to reality than modelling and the question arises, to what extent the bounds already fulfill our needs. To answer this question we return to the technological aspects I pointed out above. In this context the bound concept provides two alternatives to optimize microstructures as shown in Fig. 7: since in-situ microstructures usually refer to properties in between the bounds

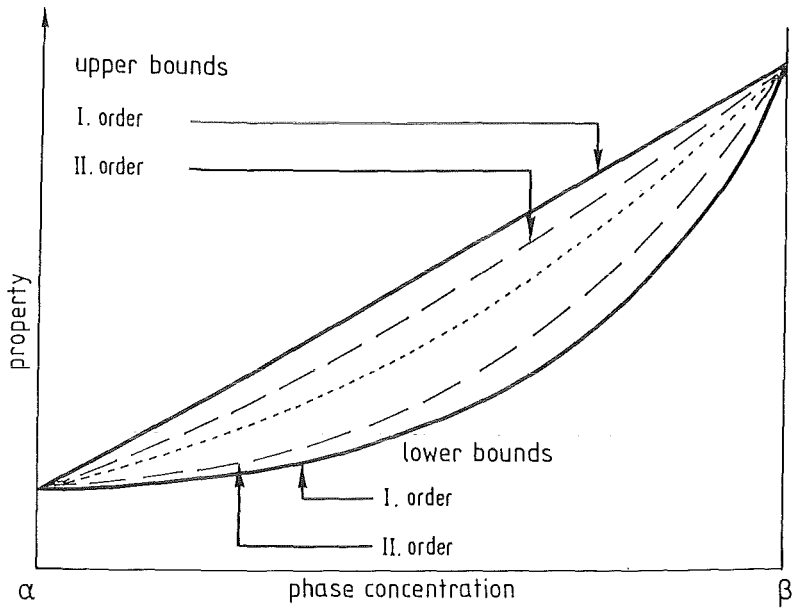

Fig. 6. I and II order bounds in curves.

- we may either save rare or ecologically risky phase materials at constant properties
- or we may achieve a higher conductivity at constant phase concentration

by microstructural constructions. Both games are the more effective, the bigger the difference is between the properties of the pure phases as for example in Fig. 8. But exactly in these cases the bound concept frequently does not provide a sufficient engineering tool to construct tailor-made materials because the bounds are far too far from each other. For porous materials the lower bounds even fail becoming zero for all porosities. This is why apart from the microstructological or general scientific interest we continue to obtain an equation providing closer bounds or even singular values, where sufficient microstructural information is available.

Model concept

On this second theoretical way, the model concept helps, leaving behind, however, the premise of no geometric assumptions. What we assume is the spheroidal substitution of the real microstructure, not been chosen, however, arbitrarily: the spheroidal model

- permits to approach real shapes on the basis of respective surface-to-volume ratios by altering the ratio of rotation axis and minor axis steadily; shapes as fibres, spheres and platelets are included (Fig. 9)

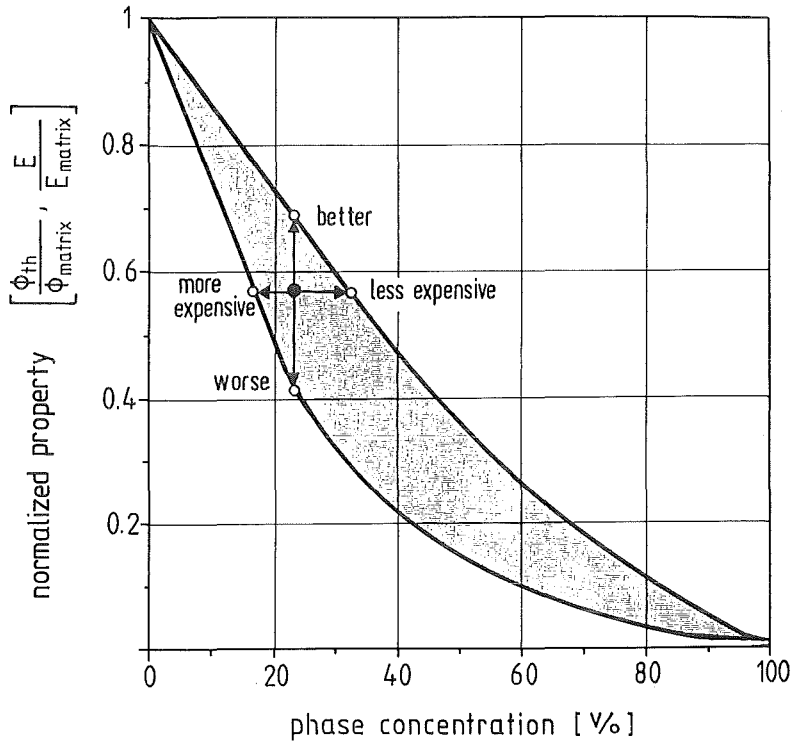

Fig. 7. Bounds and tailoring materials.

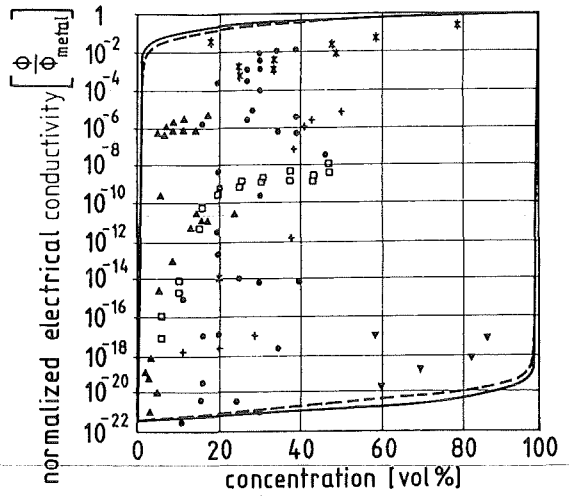

Fig. 8. Electrical conductivity of cermets.

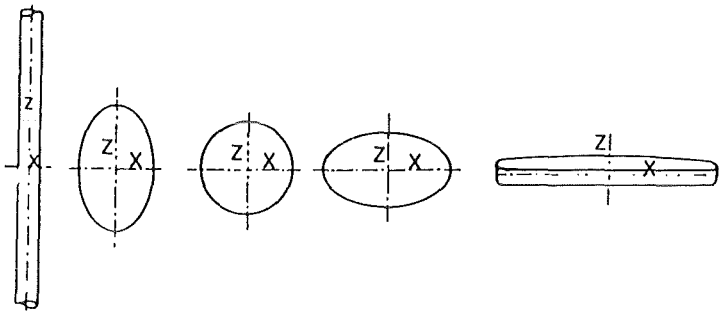

Fig. 9. Spheroidal shape variation.

- permits to calculate the respective spheroids from two-dimensional sections stereologically
- permits to calculate the stray fields induced by spheroidal inclusions.

In Fig. 10 the premises assumed for the model concept are summarized.

implicite parameters	1. number of phases	e.g. two-, three-, multiphased premise: thermochemical equilibrium
	2. type of microstructure matrix phase microstructure interconnecting phase microstructure	premise: continuum principle
explicite parameters	3. volume fraction of phase (concentration factor) volume x number of the phase particles 4. shape of phase particles (shape factor) 5. orientation of phase particles (orientation factor)	premise: - spheroidal model mean values

Fig. 10. Model concept premises.

So what we consider from now is the substitution of the real microstructure of a two phase material by a spheroidal based model microstructure with mean sized, shaped and oriented spheroidal inclusions in a matrix phase. This is what we call mean value-premise. Furthermore we assume that the continuum principle holds true for the material and that the material is in thermochemical equilibrium, that is to say, no interaction occurs at the phase boundaries.

The derivation itself, in summary, is as follows [1,3,7,8,9]: for spheroidal inclusions it is possible to calculate the respective stray field for the inclusions (Fig. 11) which depends on their shape and orientation and may be

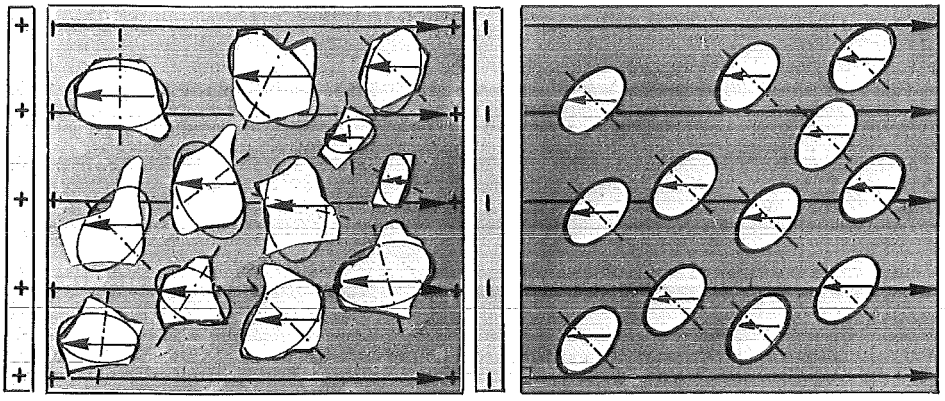

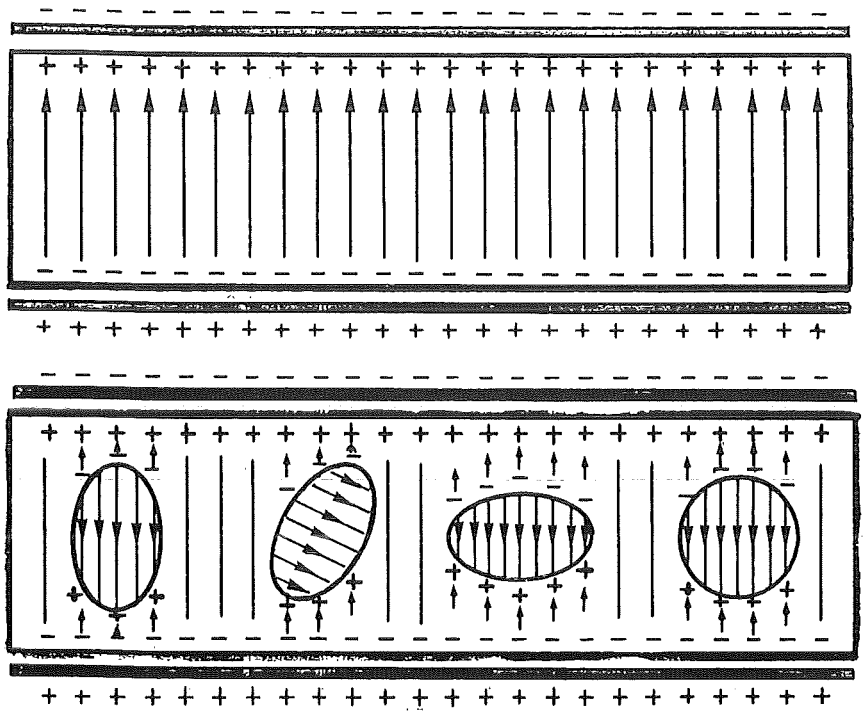

Fig. 11. Model concept schematically
- substituting of real particles by spheroids (above) -
- single phased material in a primary field (middle) -
- two-phased model material in a primary field (below) -

superimposed on the original primary field mathematically. The resulting constitutive microstructure-field property equations (general 8; simplified 9, 10) can be solved in terms of conductivity, where the effective conductivity of the two-phase material is given as a function of the phase conductivities, the phase concentration factor, the shape factor and the orientation factor

$$1-c_D = \frac{\Phi_D - \Phi_C}{\Phi_D - \Phi_M}\left[\frac{\Phi_M}{\Phi_C}\right]^h \left[\frac{\Phi_C + g\Phi_D}{\Phi_M + g\Phi_D}\right]^k \tag{8}$$

$$h, g, k = f(F_D, \cos^2 \alpha_D)$$

$$\frac{\Phi_D}{\Phi_M} << 1 : \Phi_C = \Phi_M (1-c_D)^{\frac{1-\cos^2\alpha_D}{1-F_D} + \frac{\cos^2\alpha_D}{2F_D}} \tag{9}$$

$$\frac{\Phi_D}{\Phi_M} >> 1 : \Phi_C = \Phi_M (1-c_D)^{\frac{\cos^2\alpha_D - 1}{F_D} - \frac{\cos^2\alpha_D}{1-2F_D}} \tag{10}$$

$$0 \le c_D \le 1$$

$$0 \le \cos^2 \alpha_D \le 1$$

$$0 \le F_D \le 0{,}5$$

(ϕ = field properties; C, M, D = subscripts for the two-phased material, the matrix phase, the included phase; c_D = volume content of included phase = concentration factor; F_D = shape factor of the included phase; $\cos^2 \alpha_D$ = orientation factor of the included phase.

The constitutive microstructure-field-property equation simplifies for large differences in the phase properties as for cermets or porous materials; but demonstrates generally that the effective field property of a two phase material depends on implicit microstructural parameters and explicit microstructural factors (Fig. 10).

Implicite parameters govern the type of the constitutive equation but do not appear explicitly, while the explicit factors are defined as such in the equation. I might additionally mention that I have here considered only the equations for matrix phase structures, but that an analogous equation for interconnecting phase microstructure (compare Fig. 12) is already available [10].

Knowing now about the bound concept and the model concept we have to ask for the feedback between the model equations based on geometrical assumptions and the bound equations being free from such assumptions. If, for example, the orientation factor $\cos^2 \alpha_D$ in the model equation is put to be $\frac{1}{3}$, which refers to isotropic microstructures in terms of the model and the equation is then solved with respect to the shape factor for highest and lowest effective conductivities

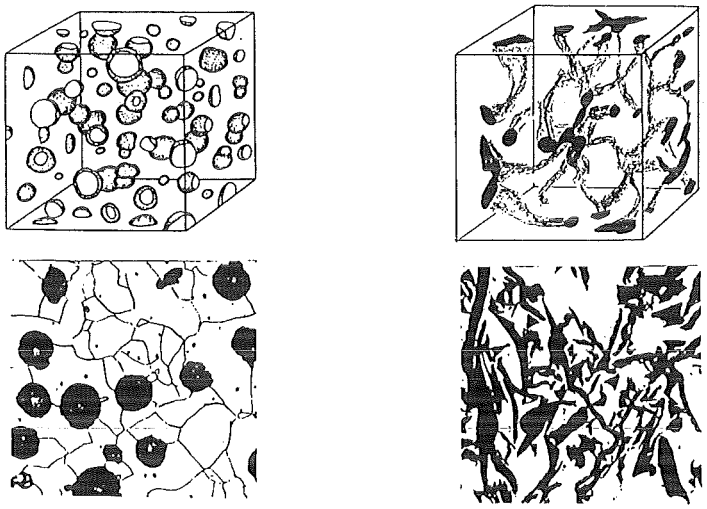

Fig. 12. Matrix and interconnecting phase microstructures.

$\cos^2\alpha_D$ → / F_D ↓	0 orientation perpendicular to the field direction	0,33 orientation statistical (isotropic) to the field direction	1 orientation parallel to the field direction
0 cylindrical disc	$1-c_D = \frac{\varphi_D-\varphi_C}{\varphi_D-\varphi_M}$ ($\hat{=}$ I. order upper bound)	$1-c_D = \frac{(\varphi_D-\varphi_C)}{(\varphi_D-\varphi_M)} \cdot \frac{(\varphi_M+2\varphi_D)}{(\varphi_C+2\varphi_D)}$ ($\hat{=}$ II. order bounds for $\varphi_D > \varphi_M$ or $\varphi_D < \varphi_M$)	$1-c_D = \frac{\varphi_D-\varphi_C}{\varphi_D-\varphi_M} \cdot \frac{\varphi_M}{\varphi_C}$ ($\hat{=}$ I. order lower bound)
0,33 sphere	$1-c_D = \frac{\varphi_D-\varphi_C}{\varphi_D-\varphi_M}\left(\frac{\varphi_M}{\varphi_C}\right)^{\frac{1}{3}}$ ($\hat{=}$ III. order upper bound)		
0,5 cylindrical fiber	$1-c_D = \frac{\varphi_D-\varphi_C}{\varphi_D-\varphi_M}\left[\frac{\varphi_M}{\varphi_C}\right]^{\frac{1}{2}}$	$1-c_D = \frac{\varphi_D-\varphi_C}{\varphi_D-\varphi_M}\left[\frac{\varphi_M+\frac{1}{5}\varphi_D}{\varphi_C+\frac{1}{5}\varphi_D}\right]^{\frac{2}{5}}$	$1-c_D = \frac{\varphi_D-\varphi_C}{\varphi_D-\varphi_M}$

Fig. 13. Table of special solutions (equations 11 - 17) of the model concept.

and if we put these two extreme shape factors into the constitutive microstructure property equation, we get two bound equations being identical with the II order bounds of the bound concept (Fig. 13). This is valid for other bounds too and is an important theoretical verification for the validity of the two concepts to the same problem. Both converge into each other as schematically demonstrated in Fig. 14. Via the model concept it became also possible to provide the missing lower bounds in the bound concept for porous materials [11,12,13].

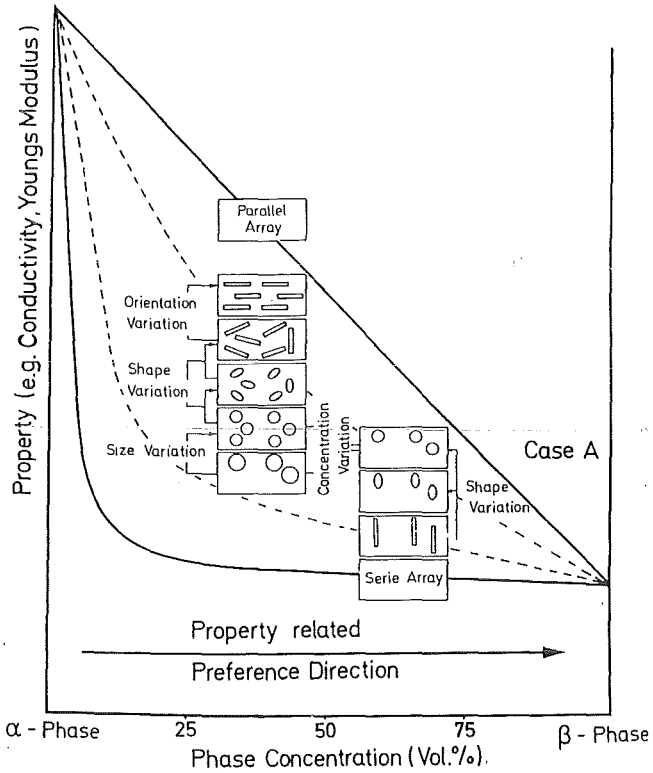

Fig. 14. Schematic bound-model convergency.

Youngs Modulus of Elasticity

Turning now to Young's modulus of elasticity we follow the same line of theoretical consideration: applying stresses to a two-phase system, which are below the yield strength of the two phases, elastic deformation takes place as a consequence of the stress-strain-field. Variational principles in theoretical mechanics permit to derive an equation providing the effective elastic deformation energy taken up by the system and its phases [14,15,16]. Again solving this energy equation for the effective elastic constants two solutions result, providing upper and lower bounds of different order (Fig. 15). I order bounds again refer to systems about which nothing else is known with respect to their microstructure than that they are formed by two phases. II. order bounds refer to two-phased and isotropic materials. In order to get definite values for a more definite microstructure theoretically again the model like characterization of the microstructure is necessary (Fig. 16). The spheroidal model chosen for the same reasons as explained for the field properties is slightly modified for the derivation: after substituting the real microstructure by the spheroi-

	lower bounds	upper bounds
I order	$E_{IC} = \frac{E_M \cdot E_D}{(1-c_D)\cdot E_D + c_D \cdot E_M}$	$E_C^I = (1-c_D)\, E_M + c_D \cdot E_D$
	$E_C = \frac{9G_C \cdot K_C}{3K_C + G_C}$	
II order	$K_{IIC} = \frac{E_M}{3(1-2\nu_M)} + \frac{c_D}{\frac{3(1-2\nu_D)(1-2\nu_M)}{E_D(1-2\nu_M)-E_M(1-2\nu_D)} + \frac{(1-c_D)(1-2\nu_M)(1+\nu_M)}{E_M(1-\nu_M)}}$	$K_C^{II} = \frac{E_D}{3(1-2\nu_D)} + \frac{1-c_D}{\frac{3(1-2\nu_M)(1-2\nu_D)}{E_M(1-2\nu_D)-E_D(1-2\nu_M)} + \frac{c_D(1-2\nu_D)(1+\nu_D)}{E_D(1-\nu_D)}}$
	$G_{IIC} = \frac{E_M}{2(1+\nu_M)} + \frac{c_D}{\frac{2(1+\nu_D)(1+\nu_M)}{E_D(1+\nu_M)-E_M(1+\nu_D)} + \frac{4(1-c_D)(4-5\nu_M)(1+\nu_M)}{15E_M(1-\nu_M)}}$	$G_C^{II} = \frac{E_D}{2(1+\nu_D)} + \frac{1-c_D}{\frac{2(1+\nu_M)(1+\nu_D)}{E_M(1+\nu_D)-E_D(1+\nu_M)} + \frac{4c_D(4-5\nu_D)(1+\nu_D)}{15E_D(1-\nu_D)}}$

Fig. 15. Bound equations (18 - 24) for Youngs modulus.

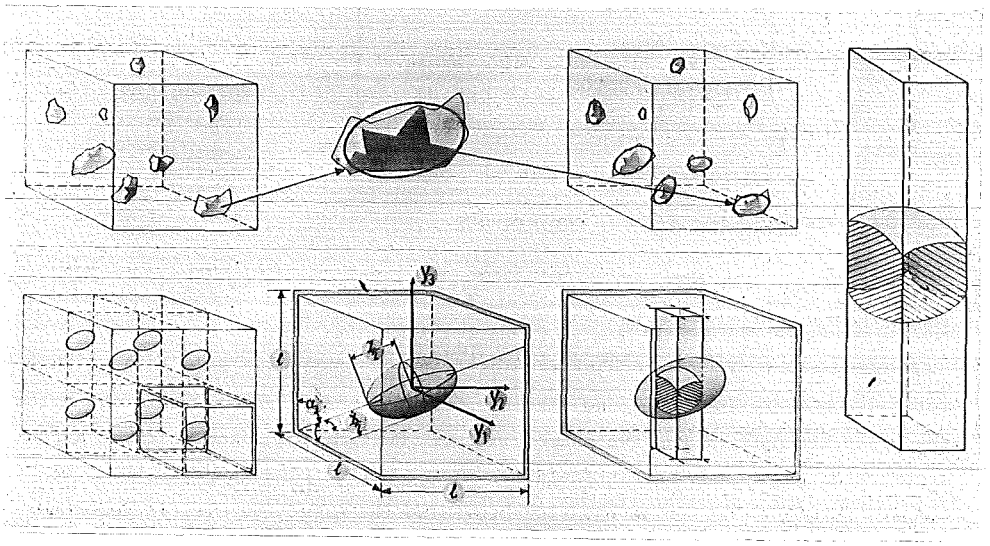

Fig. 16. Model scheme for Youngs modulus.

dal model finite elements are subdivided in small prismatic columns. In them the two phases are arranged in series with respect to the stress direction adapting by different strains the constant stress. Putting the columns together in one piece columns with different effective Youngs moduli are arranged parallel to each other. The adaptation to the external stress now results in equal strains for each column but different stresses. This mathematical procedure yields to a constitutive equation for Youngs modulus of elasticity which - as

an engineering approach - is not yet as far developed as for the conductivity but restrictiveless reliable up to about 50 % by volume of the phases [17]. Its simplified form valid for big differences between the moduli of the phases as in the case of porous ceramics for example, is

$$E_P^{(1)} = E_M \left[1 - \pi \cdot \sqrt[3]{\frac{9P^2}{16\pi^2} \cdot \frac{z}{x}} \quad \sqrt{1 + \left[\left(\frac{x}{z}\right)^2 - 1 \right] \cos^2 \alpha_D} \right] \qquad \text{(pores)} \qquad (25)$$

$$E_P^{(1)} \approx E_M \left[1 - 1{,}21\, P^{2/3} \right] \qquad \text{for } P \leq 0.5 \qquad \text{(spherical pores)} \qquad (26)$$

($E_P^{(1)}$ = Young's modulus for the porous material, 1st approach; E_M = Young's modulus for the matrix material; z_x = rotation axis and minor axis of the substituting spheroidal pores; $\frac{z}{x}$ = shape factor; P = porosity = concentration factor; $\cos^2 \alpha_D$ = orientation factor of the spheroidal pores).

Again the equations are based on two implicit parameters as the number of phases and the type of microstructure, not appearing explicitely in the constitutive microstructure-Young's modulus equation and the explicit microstructural factors for the concentration, shape and orientation of the included phase, since the here given equation refers to matrix phase microstructure.

In case of the elastic constants we have not yet verified the convergency between the bound equations and the constitutive microstructural-property-equations in general - as we did already in the case of field properties; but special cases work - and we work about the general verification also for the elastic properties.

Summarizing what I did up to this point I may conclude, that from a theoretical point of view - refusing definite geometrical assumptions for microstructure property-correlations - restricts the result to bounds of a certain degree. For the derivation of 'higher degrees' of such a correlation - as unique property values - we had to accept geometrical assumptions being, however, compatible with the less definite but assumptions free bounds of lower order. Although this is the present theoretical state-of-the-art in our work, it is not yet finally decided, that the microstructural factors in constitutive equations are undoubtedly linked to a definite geometrical model instead of becoming global microstructural parameters in the future [18]. The following consideration about how to determine microstructural factors will even more clarify, why we think so.

DETERMINATION OF MICROSTRUCTURAL FACTORS BY QUANTITATIVE MICROSTRUCTURAL ANALYSIS

As a consequence of the theoretical derivation the phase concentration factor in the constitutive microstructure-property equation refers simply to the volume fraction of one phase which - according to Delesse's principle [19,22,24,25] -

may directly be measured as areal fraction in sections through the material considered. The phase concentration factor therefore is a global microstructural parameter [18].

The more sophisticated shape factor itself is identical with the depolarization factor for field properties well known from physics when including spheroids in a homogeneous electrostatic or temperature field [21]. As such - and exclusively for spheroids - it was derived as a function of the axial ratio $\frac{z}{x}$ of the spheroid shown in Fig. 17, where z is the rotation axis generally [22].

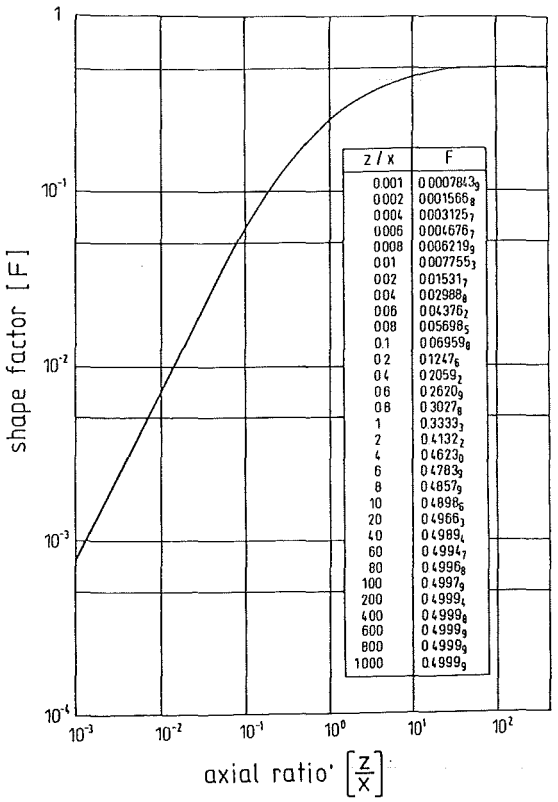

z / x	F
0.001	0.000781_3
0.002	0.001566_8
0.004	0.003125_7
0.006	0.004676_7
0.008	0.006219_9
0.01	0.007755_3
0.02	0.01531_7
0.04	0.02988_8
0.06	0.04376_2
0.08	0.05698_5
0.1	0.06959_8
0.2	0.1247_6
0.4	0.2059_2
0.6	0.2620_9
0.8	0.3027_8
1	0.3333_3
2	0.4132_2
4	0.4623_0
6	0.4783_9
8	0.4857_9
10	0.4898_6
20	0.4966_1
40	0.4989_4
60	0.4994_7
80	0.4996_8
100	0.4997_9
200	0.4999_4
400	0.4999_8
600	0.4999_9
800	0.4999_9
1000	0.4999_9

Fig. 17. Depolarization factor: shape factor.

- For Young's modulus the shape factor is more simple and refers directly to the spheroids' axial ratio [17]. The orientation factor, although expressed as cosinus of the average angle between the rotation axis and the electromagnetic or temperature field - or the stress-strain field for elastic properties - may also be determined exclusively by measured axial ratios in prescibed sample sections [22,26].

$$\cos^2\alpha_{\shortparallel} = \left[\frac{\left(\frac{z}{x}\right)^2_{\shortparallel} - \left(\frac{\overline{b'}}{a'}\right)^2_A - 1}{\left(\frac{z}{x}\right)^2_{\shortparallel} - 1} \right] \tag{27}$$

$$\cos^2\alpha_{=} = \left[\frac{\left(\frac{z}{x}\right)^2_{=} - \left(\frac{\overline{a'}}{b'}\right)^2_A - 1}{\left(\frac{z}{x}\right)^2_{=} - 1} \right] \tag{28}$$

($\cos^2\alpha_{\shortparallel}$ = orientation factor in case of prolate spheroids; $\cos^2\alpha_{=}$ = orientation factor in case of oblate spheroids; $\left(\frac{z}{x}\right)_{\shortparallel}$, $\left(\frac{z}{x}\right)_{=}$ = axial ratios of prolate and oblate spheroids, respectively; $\left(\frac{\overline{a'}}{b'}\right)_A$, $\left(\frac{\overline{b'}}{a'}\right)_A$ = averaged axial ratios of ellipses measured in section A, Fig. 18).

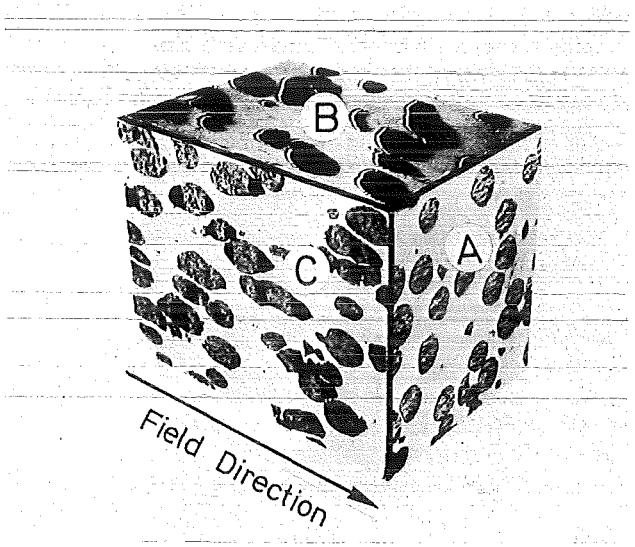

Fig. 18. Orientation factor: model explanation.

When measuring for example the axial ratios in the front section A, this quantity will change by orientation. In the picture the orientation is almost parallel to the field and therefore the areal axial ratio is 1 for circles. Changing the orientation it becomes different to one, where the difference provides the tool to calculate quantitatively the orientation factor from axial ratios by equations (27) and (28).

The actual task therefore arising from the theoretically obtained definitions of the microstructural factors is to calculate spatial as well as areal axial ratios from areal quantities measured in two-dimensional sections. This, however, may be done by stereological relationships especially available for the case of spheroids, which was one crucial reason to prefer this model.

Let us now follow for a moment the quantitative microstructural analysis in practice to make the method lucid [22,24,25,26,27]. The areal axial ratios of a real material are determined as demonstrated in Fig. 19 by measuring the area and the perimeter of the real features. The adaptation to the model is achieved by substituting the real features by ellipses with respective area-to-perimeter ratios. From them we get a mean axial ratio of the ellipses, which is transformed stereologically into the axial ratio of the respective spheroid as pointed out graphically in fig. 20 [22,26]. This, in short cut, is the principle of

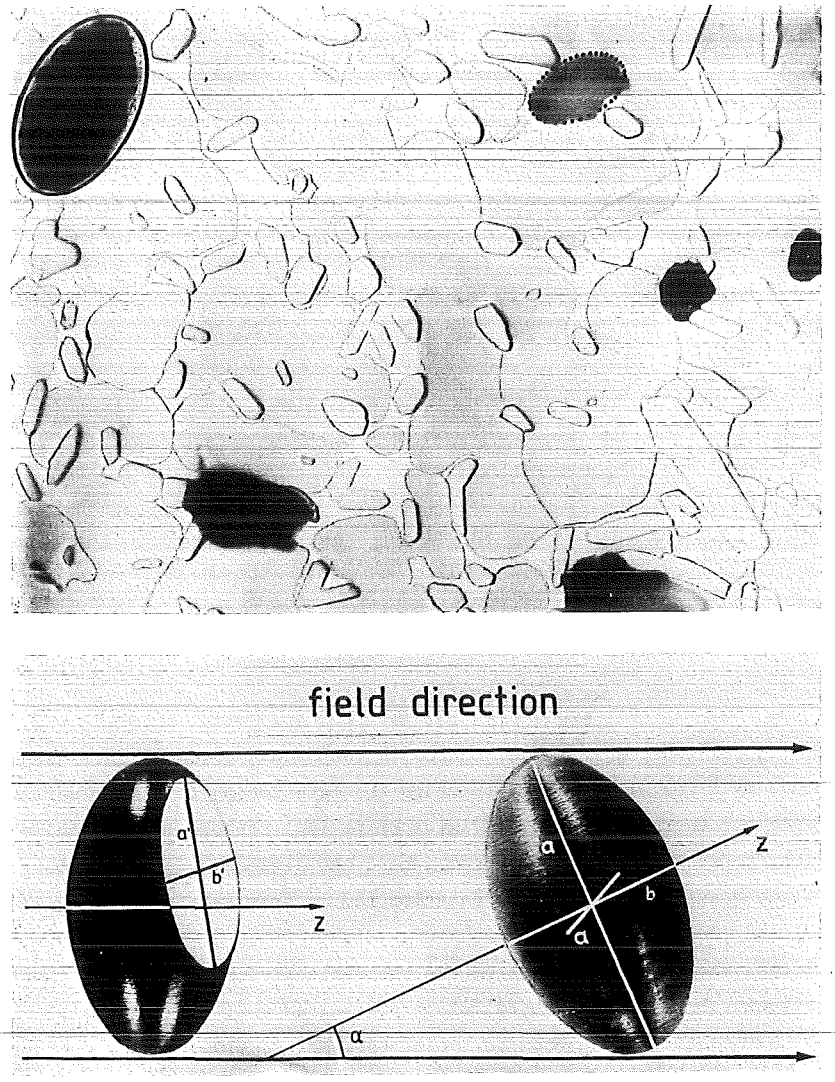

Fig. 19. Substituting ellipses in sections.

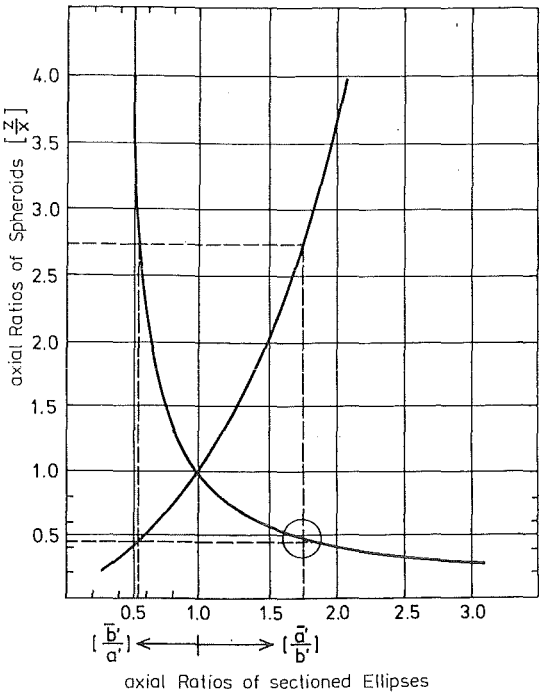

Fig. 20. Transformation of axial ratios.

deriving the microstructural factors, which result from constitutive microstructure-property-equations. Those, which are related to geometrical assumptions, altogether result from axial ratios, say ratios of lineal features. We have started meanwhile to investigate, wether we may substitute the axial ratios by a normalized intercept length. In case of success, the shape factor as well as the orientation factor would become functions of global parameters and the spheroidal model would just play the role of a fictive aid to reflect reality fairly correctly during derivation. For the moment, however, I have to let this be an open question and turn to check first the prior question, if the theoretical equations at all satisfy the demands of - at least - an engineering approach by comparing calculated and measured values of field properties and Youngs modulus for real two-phase materials.

COMPARISON OF CALCULATED AND MEASURED VALUES OF TWO-PHASE MATERIALS

In order to keep within the frame of this publication I restrict the demonstration to selected measured and calculated thermal conductivities and Youngs moduli of elasticity of two-phase metals, ceramics and composites as well as porous materials, where pores are treated as a second gaseous phase. Only a few

examples of the electrical conductivity and magnetic permeability of two-phase materials are included therefore in the following plots. Others, however, are already published in large number [10,11,12,13,23,28,29,30,31,32,33,36].

Let us first consider I order bounds for the thermal conductivity and experimental values, then continue with higher order bounds and 'singular' values and finally repeat this for Youngs modulus. In Fig. 21, I order bounds are compared with measured thermal conductivities for two-phased ceramic materials. The

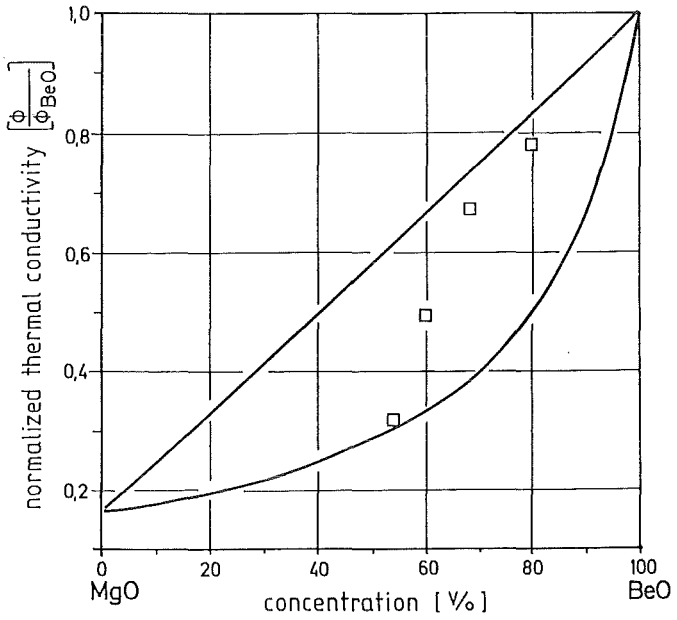

Fig. 21. MgO-BeO, I order bounds, thermal conductivity.

same is done for different cermets at different temperatures in Fig. 22. I. order bounds not only for thermal conductivities (T.C.) but also for electrical conductivities (E.C.) and magnetic permeabilities (M.P.) as well are indicated in fig. 23 together with experimental values for porous metals. In Fig. 24 the comparison is given for measured thermal conductivities of polymer-metal composites and III order bounds assuming polymer matrix phases. As comes out for some of them the presupposition is not fulfilled without exceptions However, the experimental values of thermal conductivity in Figs. 25, 26 and 27 fit into higher order bounds, where in the case of porous ceramics the majority of experimental values is bound by III order curves due to closed porosity. The rest refers to interconnected porosity. The same is valid for the thermal (T.C.) and electrical (E.C.) conductivity of porous graphite (Fig. 28).

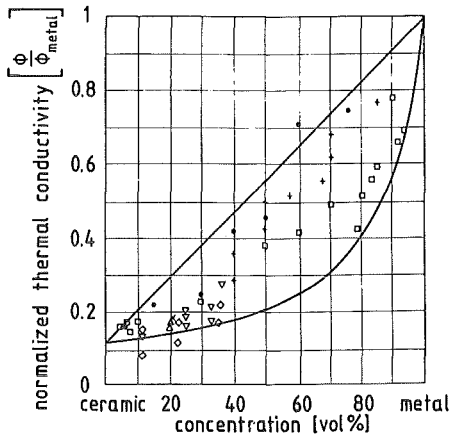

Fig. 22. Cermets, I order bounds, thermal conductivity.

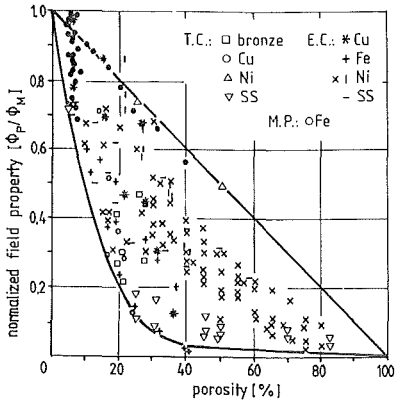

Fig. 23. Porous metals, I order bounds, field properties.

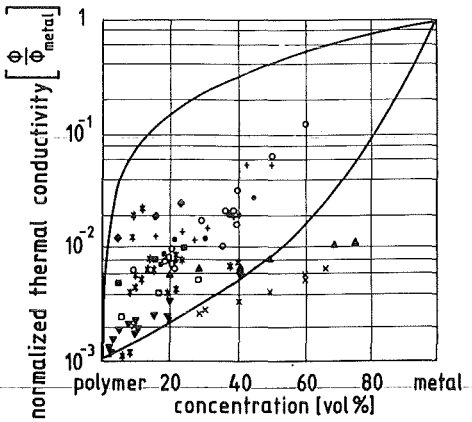

Fig. 24. Polymer-metal-composites, III order bounds, thermal conductivity.

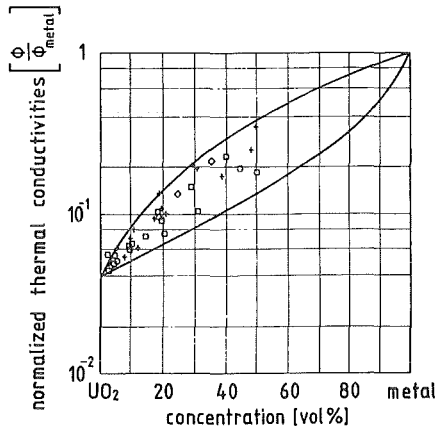

Fig. 25. Nuclear cermets, III order bounds, thermal conductivity.

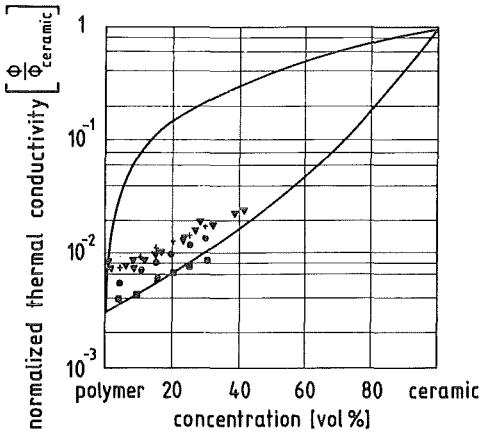

Fig. 26. Isotropic polymer-ceramic-composites, III. order bounds, thermal conductivity.

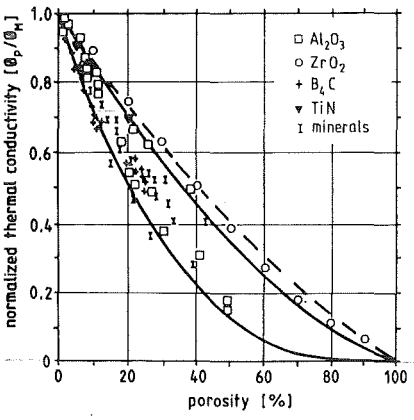

Fig. 27. Isotropic porous ceramics, II/III. order bounds, thermal conductivity.

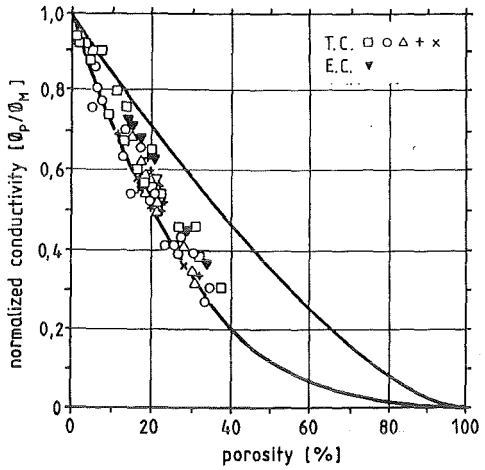

Fig. 28. Porous graphite, III order bounds, thermal conductivity.

Let us now glance at some 'singular' curves and the respective experimental thermal conductivities as given in Fig. 29 for resin matrix-metal composites, where the metal inclusions approach spherical shape or in Fig. 30, where glass spheres are embedded in polymer matrices. For spherical pores in graphite (Fig. 31) the measured and calculated thermal conductivities fit as well as for oriented graphite fibres in Fig. 32.

So much for the comparison between measured and calculated thermal conductivities.

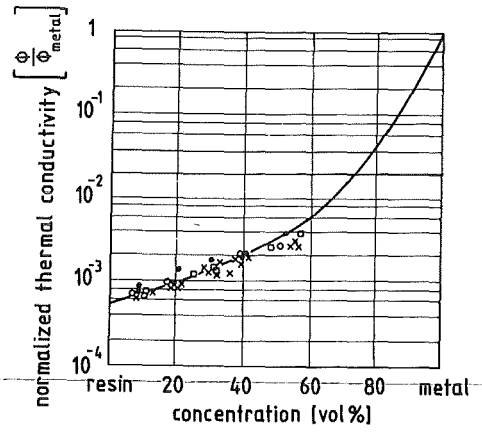

Fig. 29. Resin (matrix) -metal composites spherical inclusions.

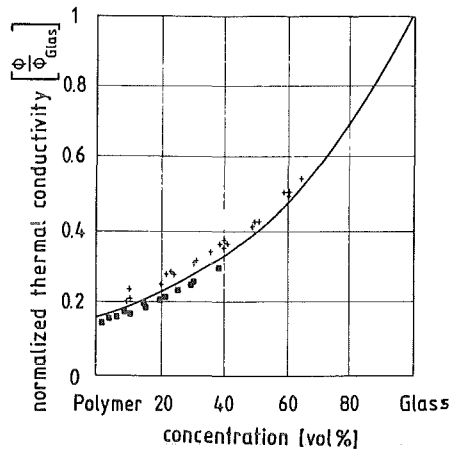

Fig. 30. Polymer matrix-glass composites spherical inclusions.

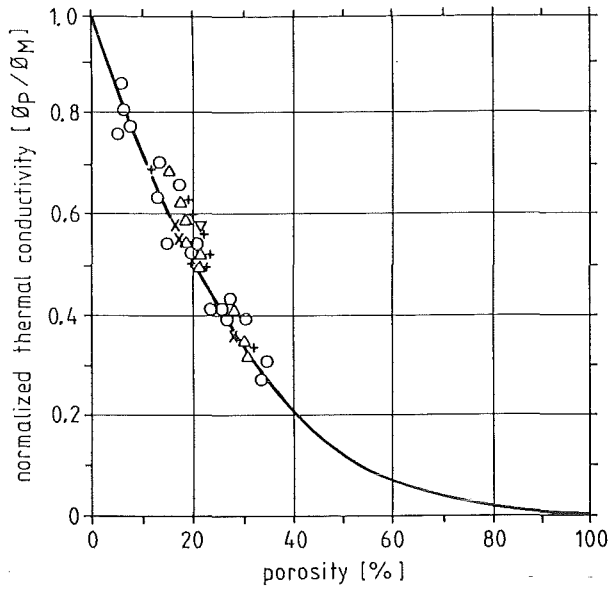

Fig. 31. Spherical porosity in graphite.

And now a few similar examples for the effective Youngs modulus of two-phased materials. In Fig. 33 we have I order bounds and the experimental values of Young's modulus for a two-phase carbide-oxide ceramic material and in Fig. 34 for a ceramic-graphite composite material. Also for porous ceramics (Fig. 35) the measured Young's moduli fit into the preliminary I. order bounds. Finally II order bounds are compared with experimental data in Fig. 36 for an isotropic two-phased silicate and in Fig. 37 for WC-Co hard metals. Least and last in

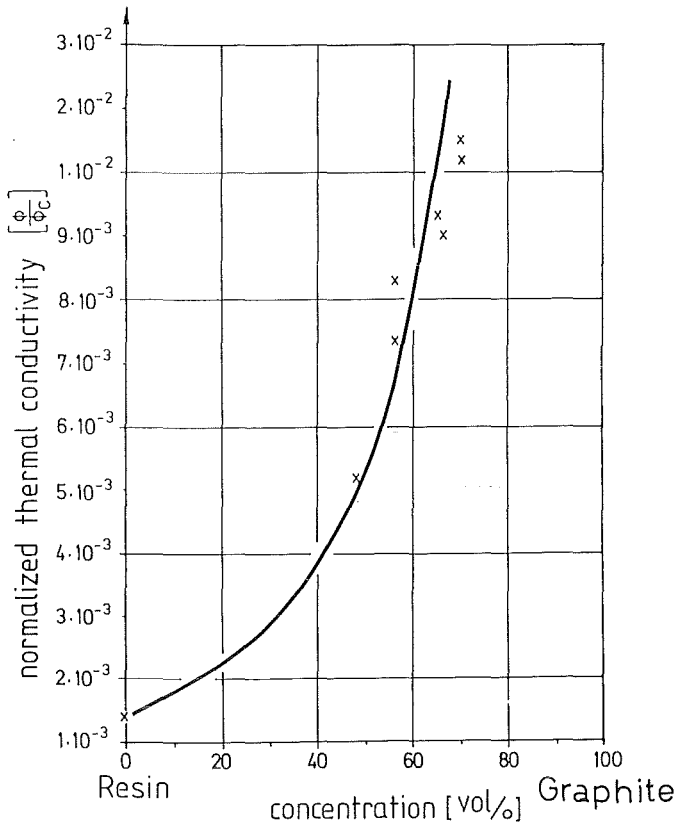

Fig. 32. Resin matrix-graphite fibres, oriented with the theoretical curves.

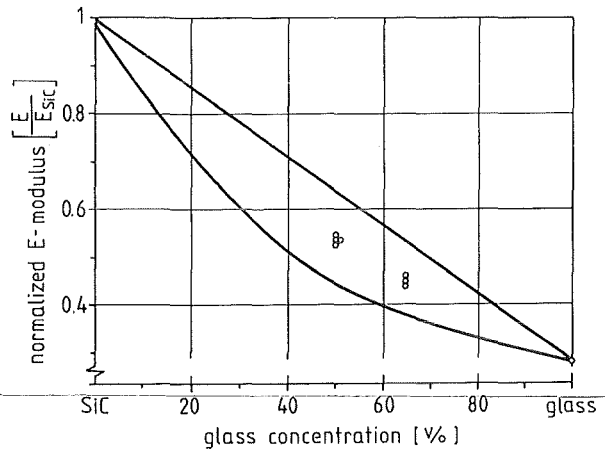

Fig. 33. SiC-glass I order.

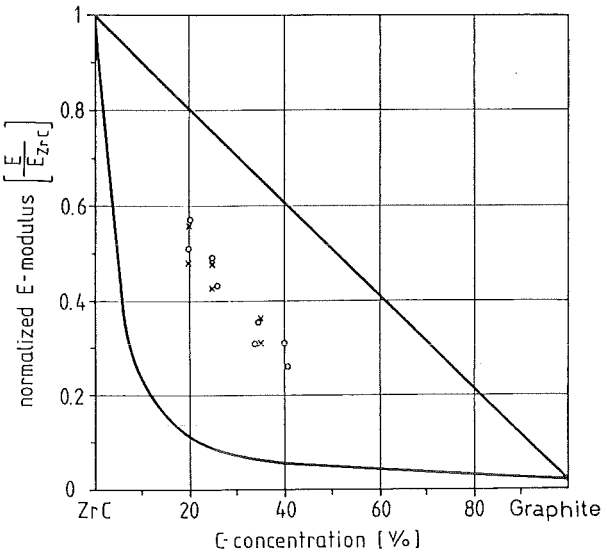

Fig. 34. ZrC-graphite, I order bounds.

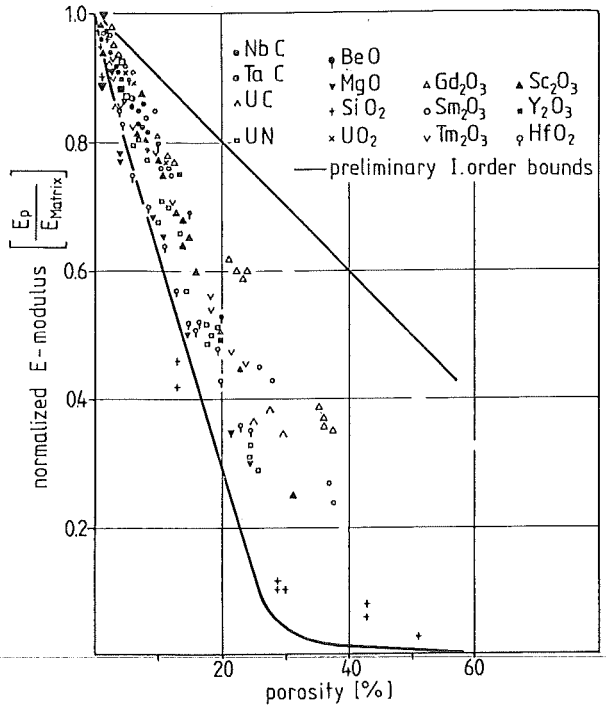

Fig. 35. Porous ceramics, I order bounds.

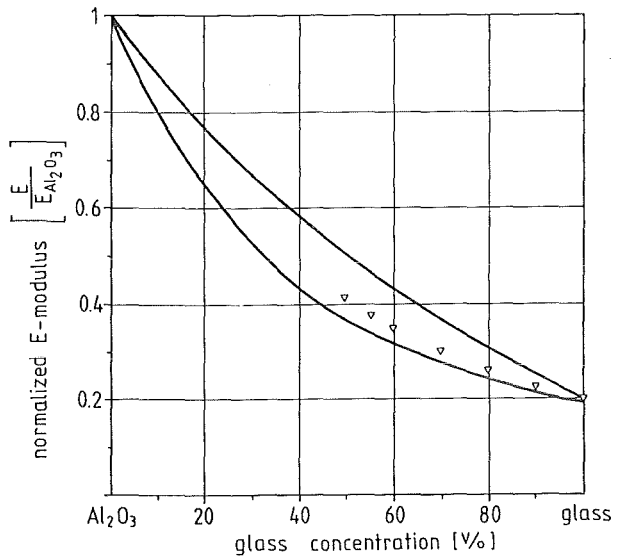

Fig. 36. Al_2O_3-glass, II order bounds.

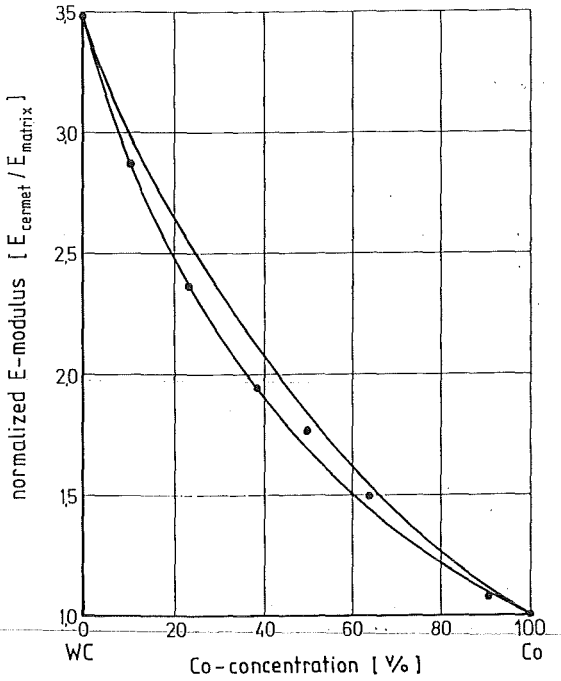

Fig. 37. WC-Co, III order bounds.

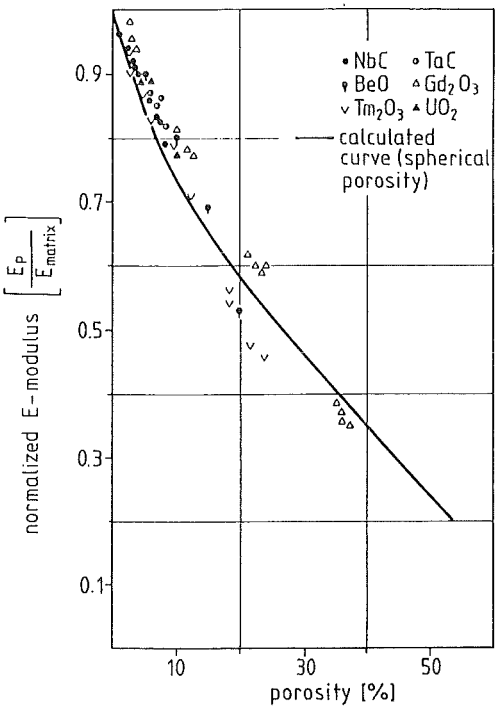

Fig. 38. Porous ceramics, spherical porosity.

Fig. 38 measured Young's moduli for porous ceramics with closed spherical porosity are compared to the respective theoretical curve, permitting the statement, that the theoretical microstructure-property correlations have passed the engineering test of comparison with experimental data.

With that more general result let me once more return to what I mentioned at the beginning by the term 'technical properties: the thermal shock resistance and their microstructural dependences. For demonstration I refer just to porous ceramics. As mentioned before the thermal shock resistance of non-porous ceramics is proportional to the rupture strength, the thermal expansion coefficient, the thermal conductivity and Young's modulus of elasticity (eq. 1) [4]. Two of these terms - conductivity and modulus - we may now substitute by porosity functions from the above constitutive microstructural property-equations. We have done it approaching spherical pores [34]

$$R_{TS}(P) = \text{const.}\ \frac{R_m(1-P)^x}{\alpha_{th}(P)} \cdot \frac{\Phi_{th}(1-P)^{3/2}}{E(1-1.21\cdot P^{2/3})}\cdot(1-\nu) = \underbrace{\text{const.}\ \frac{R_m}{\alpha_{th}}\cdot\frac{\Phi}{E}\cdot(1-\nu)}_{R_{TS}}\cdot\frac{(1-P)^{3/2+x}}{1-1.21\cdot P^{2/3}} \qquad (29)$$

$$\frac{R_{TS}(P)}{R_{TS}} = \frac{(1-P)^{3/2+x}}{1-1.21\cdot P^{2/3}} \qquad \text{(spherical porosity)} \qquad (30)$$

In eqn. (30) a possible porosity influence on Poisson's ratio is neglected. The thermal expansion coefficient of porous materials does not depend on porosity [35] and the rupture strength although unknown as a quantitative function of porosity in form of a microstructure-property-equation, empirically follows an exponential equation

$$R_m(P) = R_{mP} \approx R_m(1-P)^x \qquad (31)$$

where x is 1 just taking into account the reduction of cross section by pores, but where x usually becomes > 1 due to stress concentrations ($x \approx 2$ for spherical pores).

In plots we get for the various terms of thermal shock resistance as a porosity function what is shown in Fig. 39 (compare eqn. 29). As you may notice, the ratio of thermal conductivity/Youngs modulus controls the degree of compensation for the rupture strength term and leads to the slope of the thermal shock resistance curve versus spherical porosity as shown in Fig. 40. There the theoretical curve is calculated assuming $x = 1$ in eq. (30). In reality due to $x > 1$ the maximum of thermal shock resistance is to be expected at lower porosities and with different heights, as - indeed - is demonstrated by experimental values for porous glass in Fig. 41. Assuming now we fill the pores of the porous ceramic by metal inclusions achieving interface bonding between them, the ratio of thermal conductivity/Youngs modulus increases rapidly with the metallic filler, whilst the other terms change little. As an example this situation is given for SiC-Si cermets in Fig. 42 as function of definite microstructure (spherical) versus Si-concentration. The resulting tentative slope for the thermal shock resistance of SiC-Si-cermets predicts fairly well real values for silicon infiltrated silicon carbide, which for about 15 vol.% silicon provides approximately a 20 % improved thermal shock resistance. The thermal shock resistance of present day Si-SiC-composites is already even higher since by excellent wettability between the phases silicon forms the matrix phase already at low concentrations.

This is what we do in order to get a better insight into the materials behaviour by microstructure-property-correlations and to use these correlations to improve this behaviour, as for example to ductilize brittle ceramics.

ACKNOWLEDGEMENTS

Mrs. Jutta Howell has thouroughly typed the manuscript, Mrs. Vera Karcher prepared the illustrations. The author gratefully appreciates this assistance.

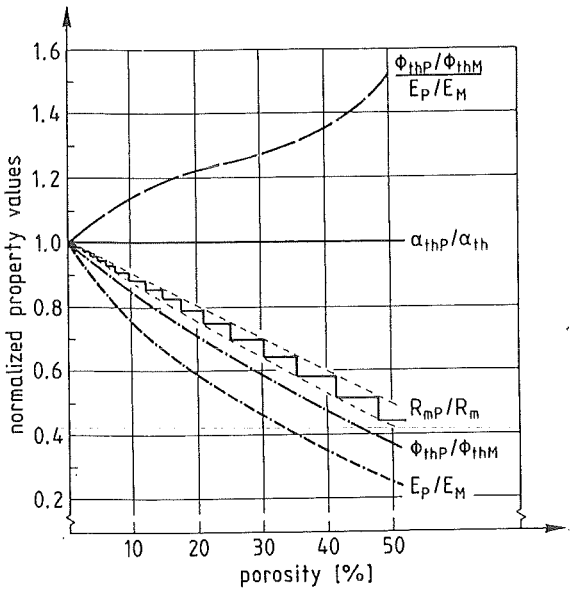

Fig. 39. Terms of thermal shock resistance as porosity functions for spherical porosity.

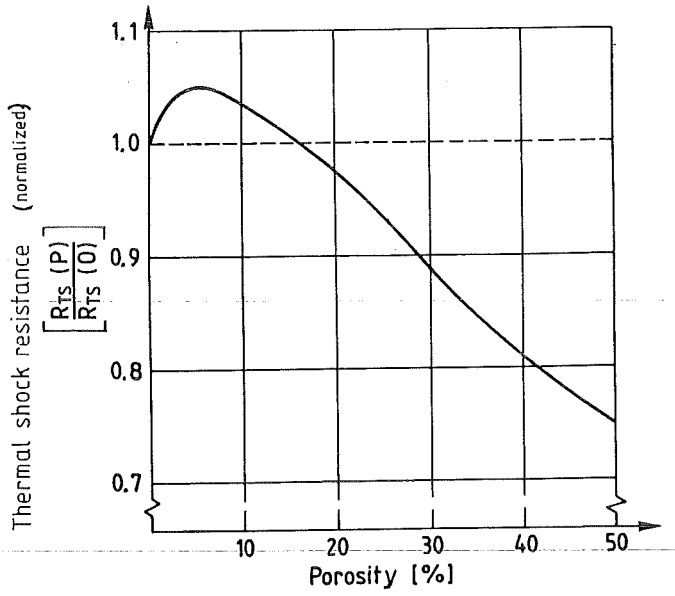

Fig. 40. Thermal shock resistance and spherical porosity.

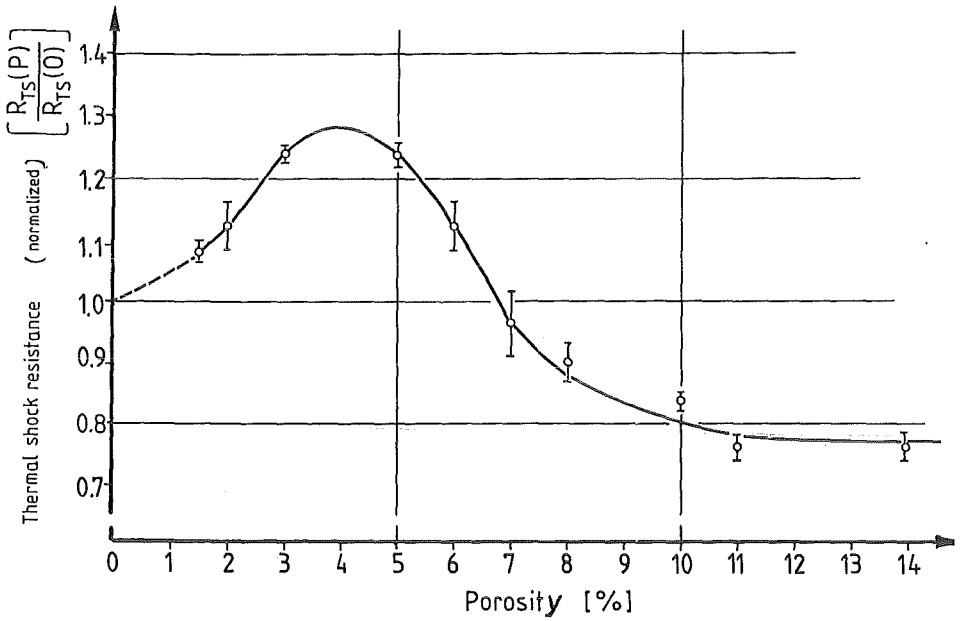

Fig. 41. Thermal shock resistance of porous borosilicate glass.

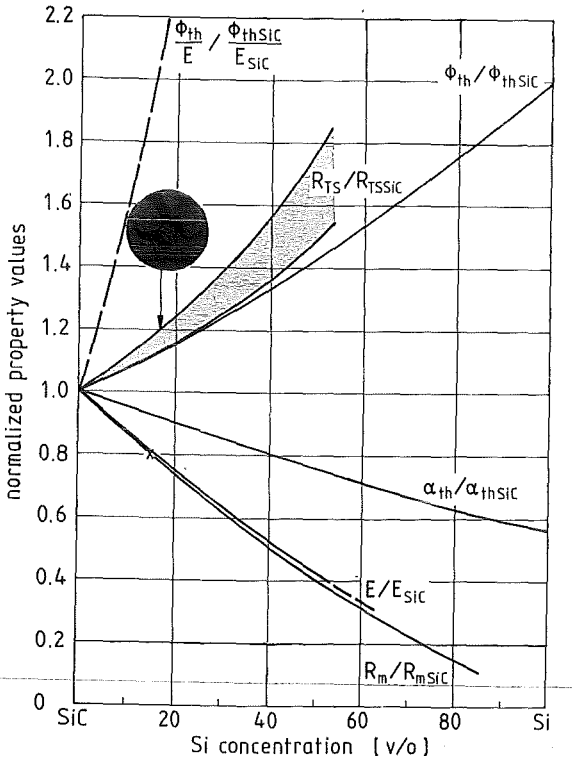

Fig. 42. SiC-Si-thermal shock resistance.

REFERENCES

1 G. Ondracek, Metall, 36-5 (1982) 523.

2 G. Ondracek, Z. Werkstofftechnik, 8-7 (1977) 240.

3 B. Schulz, Dissertation Universität Karlsruhe, (1974).

4 D.P. Hasselmann, Ceramic Bulletin, 49-12 (1970) 1033.

5 Z. Hashin and S. Shrikman, J. Appl. Phys., 33-10 (1962) 3125.

6 E. Kröner, J. Phys. F: Metal Phys., 8-11 (1978) 2261.

7 J.C. Maxwell, Treatise on Electricity and Magnetism, Oxford, Vol. I, 1904, p. 435.

8 D.A.G. Bruggeman, Ann. Phys., 24 (1935) 636; 25 (1936) 645.

9 W. Niesel, Ann. Phys., 6-10 (1952) 336.

10 B. Schulz, High Temperatures - High Pressures 13 (1981) 649.

11 P. Nikolopoulos and G. Ondracek, Proc. Int. Powder Metallurgy Conf. Florence, (1982) 89 and Z. Metallkunde, 74-1 (1983) 49.

12 P. Nikolopoulos and G. Ondracek, J. Am. Ceram. Soc., 66-4 (1983) 238.

13 P. Nikolopoulos and G. Ondracek, J. Nucl. Mat., 114 (1983) 231.

14 Z. Hashin and S. Shrikman, J. Mech. Phys. Solids, 10 (1962) 335; 11 (1963) 127.

15 Z. Hashin in R.M. Fulrath and J.A. Pask (eds.), Ceramic Microstructures, Proc. 3rd Berkeley Int. Mech. Conf., 1966, p. 313.

16 Z. Hashin, Int. J. Eng. Sci., 7 (1969) 11.

17 P. Mazilu, G. Ondracek and H. Windelberg, Internal Report, to be published (1987).

18 F.N. Rhines, Microstructology, Dr. Riederer Verlag Stuttgart (1986).

19 E.E. Underwood, Quantitative Stereology, Addison Wesley Publ. Company Inc., Reading Mass., 1970.

20 G. Ondracek, Werkstoffkunde, expert-Verlag Sindelfingen (1986)

21 U. Stille, Archiv Elektrotechnik, 30-3/4 (1944) 91.

22 G. Ondracek, Metall, 36-12 (1982) 1288.

23 G. Ondracek, Werkstofftechnik, 9 (1978) 31,96.

24 G. Ondracek, in S.L. Chermant, Practical Metallography, Special Issue, 8 (1978) 103.

25 G. Ondracek, Science in Ceramics, 6 (1973) III/1.

26 R. Pejsa, Dissertation, Universität Karlsruhe (1981).

27 G. Ondracek, R. Pejsa, J. Microscopy, 107-3 (1976) 335.

28 G. Ondracek, Werkstofftechnik, 5-8 (1974) 416; UCRL-Trans-11115 (1976).

29 G. Ondracek, Werkstofftechnik, 8-8 (1977) 280.

30 P. Klein, G. Ondracek, Revue de Chimie Minerale, 18 (1981) 392.

31 G. Ondracek, Proc. Int. Pulvermet. Tagung Dresden Vol. 2 (1981) 241; Vol. 2 (1985) 179.

32 G. Ondracek, Metall, 37/10 (1983) 10/6.

33 B. Ebel, D. Jeulin and G. Ondracek, Proc. MRS-Europe Strassburg (1985) 187.

34 U. Jauch and G. Ondracek; Werkstofftechnik, 17-9 (1986) in print.

35 S. Nazare and G. Ondracek, Werkstofftechnik, 9 (1978) 140.

36 G. Ondracek, Z. Metallkunde, 77-9 (1986) in print.